Numerical evaluation of land subsidence induced by groundwater pumping in Shanghai

Shui-Long Shen and Ye-Shuang Xu

Abstract: To predict the future behavior of land subsidence in Shanghai due to pumping of groundwater, a numerical model is established. In the proposed model, groundwater flow in three-dimensional conditions and soil deformation in one-dimensional conditions are calculated. The model takes into account the multi-aquifer-aquitard hydrogeological condition of the soft deposit of Shanghai. The variation of the coefficient of compressibility and coefficient of hydraulic conductivity of the soils with the consolidation process are simulated. Relationships among land subsidence, groundwater withdrawal volume, and groundwater level are analyzed. Comparison between the measured value and calculated value shows that the model simulates the measured value fairly well. The future of land subsidence behavior due to groundwater withdrawal is predicted and discussed via consideration of the variation of the following parameters in the future 30 years: net withdrawn volume of groundwater, pumping layer, and pumping region.

Key words: groundwater pumping, land subsidence, three-dimensional groundwater seepage, one-dimensional consolidation, prediction.

Résumé : Un modèle numérique est proposé afin de prédire le comportement futur d'un affaissement de sol causé par le pompage de l'eau souterraine à Shanghai. Dans le modèle proposé, l'écoulement de l'eau souterraine en trois dimensions et la déformation du sol en une dimension sont calculés. Le modèle considère la condition hydrogéologique multi-aquifère-aquitard du dépôt mou de Shanghai. Les variations du coefficient de compressibilité et du coefficient de conductivité hydraulique des sols lors du processus de consolidation sont simulées. Les relations entre l'affaissement du sol, le volume de retrait de l'eau souterraine et le niveau phréatique sont analysées. Des comparaisons entre les valeurs mesurées et calculées montrent que le modèle peut simuler les valeurs mesurées relativement bien. Le comportement futur du sol en affaissement causé par le retrait de l'eau souterraine est prédit et discuté en considérant les variations pour les prochains 30 ans pour les paramètres suivants : le volume net d'eau souterraine retiré, la couche de pompage et la région de pompage.

Mots-clés : pompage de l'eau souterraine, affaissement du sol, écoulement de l'eau souterraine en trois dimensions, consolidation en une dimension, prédiction.

[Traduit par la Rédaction]

Introduction

Shanghai is located near the estuary of the Yangtze River and is surrounded by Jiangsu Province and Zhejiang Province to the north and west, Hangzhou Bay in the south, and the East China Sea in the east, as illustrated in Fig. 1 (Xu et al. 2009*a*). The land region of Shanghai is a deltaic deposit of the Yangtze River with an area of about 6340 km^2. The elevation of the ground surface of Shanghai ranges from 2.2 to 4.8 m above sea level, and the elevation of the eastern part is slightly higher than that of the western part (SGEAEB 2002). The quaternary soft deposit of Shanghai is composed of rechargeable aquifers and aquitards with low hydraulic conductivity. This formation of the groundwater system in Shanghai is a so-called multi-aquifer-aquitard system (MAAS) (Xu et al. 2009*a*). The thickness of the soft deposit ranges from 100 to 300 m with a maximum of about 400 m. High quality groundwater is buried in the deeper aquifers (Lu 1994; SGEAEB 2002; Gong 2009). The first deep well recorded in official documents to withdraw groundwater for domestic use was installed in 1860 (SGEAEB 2002). With the development of industry, groundwater from aquifers to be extracted for industrial use has gradually increased since 1921 (SGEAEB 2002; Xu et al. 2008). Measurement and monitoring of the land subsidence in Shanghai started in 1921, and up to the present, the maximum recorded accumulative subsidence has reached 3 m. To control the subsidence in Shanghai, limitation of net withdrawn volume has been conducted since the mid-1960s (SGEAEB 2002; Chai et al. 2004; Xu et al. 2008). Subsidence was controlled within the allowable value till to the mid-1980s. However, since 1989, the rate of subsidence increased again and caused serious infrastructure problems (Chai et al. 2004; Gong 2009; Xu et al. 2009*a*).

To predict and (or) prevent subsidence, various prediction methods on land subsidence have been proposed (e.g., statistical method (Hozler et al. 1984), one-dimensional (1D) numerical method (SGO 1976; Qian and Gu 1981; Chai et al. 2005), quasi three-dimensional (3D) seepage method (Harada and

Received 26 March 2010. Accepted 19 July 2011. Published at www.nrcresearchpress.com/cgj on 1 September 2011.

S.-L. Shen and Y.-S. Xu. Department of Civil Engineering, Shanghai Jiao Tong University and State Key Laboratory of Ocean Engineering, Shanghai 200240, China.

Corresponding author: Ye-Shuang Xu (e-mail: xuyeshuang@sjtu.edu.cn).

Fig. 1. Plan view of district division of Shanghai Administration Region and location of cross section (modified from Xu et al. 2009*a*).

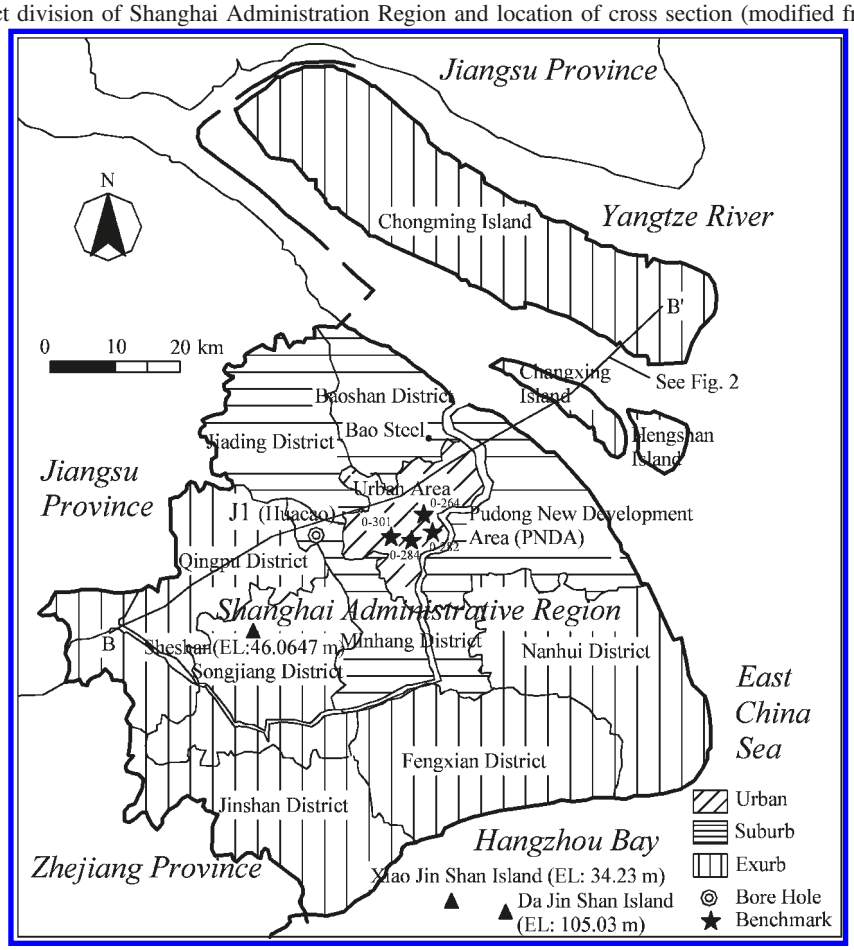

Yamanouchi 1983; Giao and Ovaskainen 2000; Li et al. 2000), and model based on 3D groundwater seepage (Gambolati and Freeze 1973; Shen et al. 2006; Xu et al. 2007)). Prediction of land subsidence in Shanghai started 30 years ago (SGO 1976). Qian and Gu (1981) employed 1D consolidation theory to calculate the subsidence in Shanghai. Li et al. (2000) presented a quasi-3D model to predict land subsidence and exploitable volume of groundwater, in which groundwater seepage in aquifer is simulated in two-dimensional (2D) condition horizontally and compression of aquitards is simulated in 1D vertical consolidation. Shi et al. (2008) presented a coupled two step model to predict the subsidence via considering the groundwater seepage in 3D and compaction in 1D. Chai et al. (2005) considered the subsidence at one place in Shanghai due to drawdown of the groundwater level and predicted future subsidence by assuming the several drawdown scenarios. In Chai et al.'s (2005) analysis, coupled 1D consolidation analysis was adopted, in which soft clay in aquitards was simulated in a modified Cam-clay model. When the calculated results were compared with the field data, the results show that the predicted results can simulate the field measured values well. However, 1D simulation can only obtained the result at one point and cannot obtain the spatial distribution of groundwater seepage and land subsidence over all the area of Shanghai. Moreover, the distribution of pumping wells cannot be simulated.

The objective of this study is to predict the future possible land subsidence in Shanghai using numerical analysis according to assumed scenarios of groundwater pumping. The numerical model incorporates 1D consolidation into a 3D seepage model of groundwater flow. Prediction on the future land subsidence is conducted via considering the variation of the volume of groundwater, pumping layer, and pumping region through reallocation of pumping wells.

MAAS in Shanghai

In accordance with marine transgression and tectonic movement during the Holocene era, Shanghai gradually took its shape as a flat coastal plain (SGEAEB 2002; Xu et al. 2009*a*). The elevation of the ground surface ranges from 2.2 to 4.8 m (based on the Wusong elevation system), and the elevation of the eastern part is a little higher than that of the western part (SGO 1979; SGEAEB 2002). The geomorphology is basically an alluvial plain. There exist some residual bedrock outcrops, which scatter in isolated hills at the southwest part, and the bedrock outcrops have a total area of about 2.5 km^2 (SGEAEB 2002; Xu et al. 2009*a*). Most of the bedrock is buried under quaternary sediments more than 300 m deep. Figure 2 shows the sectional view of the Shanghai MAAS (Xu et al. 2009*a*). As shown in this figure, the Shanghai MAAS is composed of a phreatic aquifer group (hereinafter labeled Aq0), which includes a phreatic aquifer

Fig. 2. Sectional view of hydrogeological profile of Shanghai (modified from Xu et al. 2009*a*).

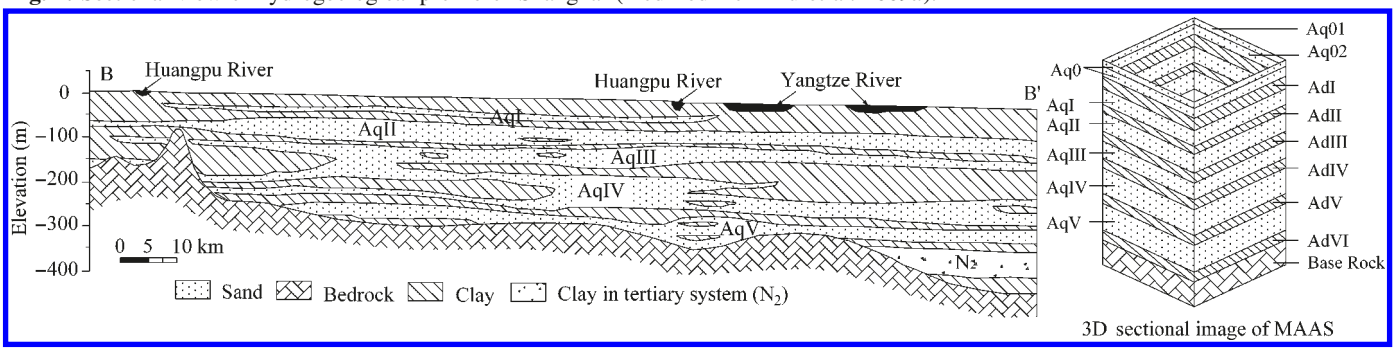

(hereinafter labeled as Aq01) overlying a low-pressure artesian aquifer (hereinafter labeled as Aq02), and five confined aquifers (hereinafter labeled AqI–AqV). Aquifers are separated by six aquitards (hereinafter labeled AdI–AdVI). Soft deposits are mainly composed of clay, silt, and sand, which has gradually accumulated during the quaternary and tertiary eras (since three million years B.P. (Xu et al. 2009*a*)). Most of the bedrock is impermeable igneous rock, which is part of the Neogene Formation. However, in some locations there is limestone with fissures, which makes the bedrock water-bearing (SGEAEB 2002; Xu et al. 2009*a*). Based on the data reported by the Shanghai Geology Office (SGO 1976; 1979), an illustrative soil profile with some available physical and mechanical properties is given in Fig. 3 (Chai et al. 2004; Xu et al. 2009*a*). Values of hydraulic conductivity given in Fig. 3 are determined from oedometer tests as recommended reference values by the Shanghai Construction and Management Commission for site investigation in Shanghai (SCAMC 2002). The detailed description on the properties of each aquifer and aquitard can be found in previous publications by the authors (Xu et al. 2009*a*, 2009*b*).

Groundwater withdrawal and land subsidence in Shanghai

Groundwater from aquifers has been extracted for industrial and domestic use since 1860 in Shanghai. Table 1 tabulates the amount of withdrawn volume of groundwater and stages of subsidence in Shanghai. Figure 4 illustrates the distribution of deep wells for groundwater withdrawal during the period from 1949 to 1963 (Zhang and Wei 2005). Figure 5 illustrates the distribution of groundwater withdrawal wells during the period from 1990 to 2000 (SGEAEB 2002; Xu 2010). Figure 6 shows the surface subsidence curves since 1921 for some benchmarks at the center of Shanghai. Locations of the benchmarks are shown in Fig. 1. Figure 7 gives the amount of groundwater pumped and recharged from 1961 to 2006. Before 1965, the subsiding rate was fast, and after 1965, the subsiding rate was reduced dramatically. Comparing Fig. 6 with Fig. 7, it can be seen that the dramatic reduction of the subsiding rate corresponds to a significant reduction in the groundwater pumping rate (Chai et al. 2004). Figure 8 shows the amount of groundwater pumped from each aquifer in Shanghai. Before 1965, groundwater was mainly pumped from AqII and AqIII. After 1965, the layers of groundwater pumping were shifted to AqIV and AqV based on the thought that the compressibility of the deeper soil layers is lower than that of the upper layers. Variation of the volume of groundwater pumped from each aquifer resulted in a change in groundwater level in each aquifer. The aforementioned description gives a rough picture of the rate of land subsidence, net groundwater pumping volume, and the water level in each aquifer.

Analytical method

Consolidation due to change in effective stress

Based on the effective stress concept (Terzaghi 1925), total stress, effective stress, and hydraulic head have the following relationship:

$$[1] \qquad \sigma' = \sigma - \gamma_w H$$

where σ' is the effective stress; σ is the total stress; γ_w is the unit weight of water; H is the hydraulic head.

When the groundwater head is drawdown, σ' will change with the hydraulic head.

$$[2] \qquad d\sigma' = d\sigma - \gamma_w dH$$

Based on Terzaghi's 1D consolidation theory, during withdrawal and (or) recharge of groundwater from an aquifer, total vertical pressure is constant and thereby

$$[3] \qquad d\sigma' = -\gamma_w dH$$

The relationship between the stress increment and the strain increment is express as

$$[4] \qquad d\varepsilon = -m_v d\sigma'$$

where m_v is the the coefficient of volume compressibility of the soil.

Combining eqs. [3] and [4], the following relationship between strain change and change of hydraulic head with time is obtained:

$$[5] \qquad \frac{\partial \varepsilon}{\partial t} = \gamma_w m_v \frac{\partial H}{\partial t}$$

As shown in eqs. [3]–[5], the withdrawal of groundwater results in drawdown of the aquifer water table, decrease of hydraulic head, and increase in effective stress. Consequently, consolidation occurs, and when the consolidated compression is transferred to the ground surface land subsidence happens.

Fig. 3. Illustration of soil profile of Shanghai (modified from Chai et al. 2004). w_n, water content; w_l, liquid limit; w_p, plastic limit; γ_t, unit weight; e_0, void ratio; C_c, compressive index; k_v, hydraulic conductivity in vertical direction.

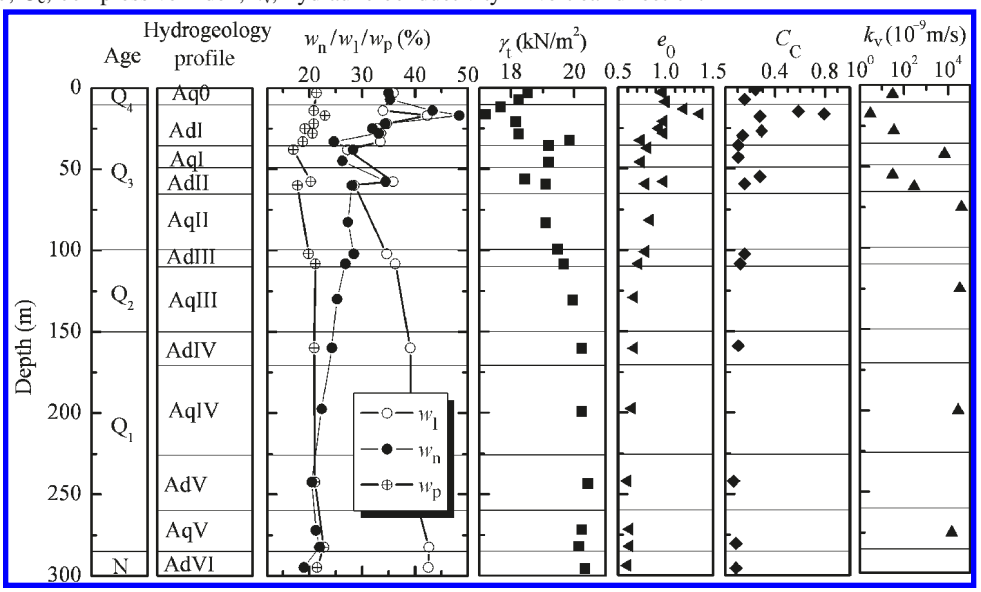

Table 1. Development of land subsidence and groundwater pumping in Shanghai (data from SGO 1976; SGEAEB 2002).

Land subsidence and groundwater pumping period					
Years	Stage	Phase	R_{st}	A_s	V_g
Developing period 1921–1965					
1921–1948	Subsidence development; groundwater initial pumping	—	22.8	19.3	9
1949–1965	Subsidence accelerated; groundwater sufficient utilization	Acceleration (1949–1956)	40.3	26.7	104
		Serious (1957–1961)	98.6	92.8	176
		Alleviation (1962–1965)	59.3	No new increase	156
Controlled period 1966–2005					
1966–1971	Slightly rebound; pumping reducing and recharging	—	–3	No new increase	71
1972–1989	Slightly subsidence; pumping aquifer adjusting	—	3.5	No new increase	105
1990–2005	Subsidence acceleration; pumping area changing	—	15	Expand to suburb	140

Note: R_{st}, average subsiding rate (mm/year); A_s, area of subsidence > 500 mm (km^2); V_g, average amount of groundwater pumping ($\times 10^6$ m^3/year).

Governing equation of groundwater flow

The governing equation for the seepage in a porous medium is denoted (Gambolati and Freeze 1973)

$$[6] \qquad \nabla(\boldsymbol{K}_{ij}\nabla H) - q = \gamma_w n\beta\frac{\partial H}{\partial t} + \frac{\partial \varepsilon}{\partial t}$$

where ∇ is the Laplace operator; $\boldsymbol{K}_{ij}$ is the tensor of hydraulic conductivity, $i, j = 1, 2, 3$; q is the source–sink flux; n is the porosity, $n = e/(1+e)$ where e is the void ratio; β is the coefficient of volumetric compressibility of water; ε is the strain; t is time.

Substituting eq. [5] into eq. [6], the governing equation for 3D groundwater flow becomes (Bear 1979; Shen et al. 2006)

$$[7] \qquad \nabla(\boldsymbol{K}_{ij}\nabla H) - q = \gamma_w(n\beta + m_v)\frac{\partial H}{\partial t} = S_s\frac{\partial H}{\partial t}$$

where $i, j = 1, 2, 3$; S_s is the coefficient of specific storage.

The coefficient of specific storage, S_s, is denoted

$$[8] \qquad S_s = {}_w(m_v + n)$$

Under the condition that the pressure of groundwater is not high, the compression of water can be ignored because the compression of water is very small compared with the compression of soil, or $\beta = 0$. Therefore,

$$[9] \qquad S_s \approx \gamma_w m_v$$

Subsidence calculation

Compression of soil layers with time can be obtained from Terzhaghi's 1D consolidation equation as expressed

$$[10] \qquad \frac{\partial u}{\partial t} = \frac{k}{m_v\gamma_w}\frac{\partial^2 u}{\partial z^2} = C_v\frac{\partial^2 u}{\partial z^2}$$

Fig. 4. Distribution of pumping wells from 1949 to 1963.

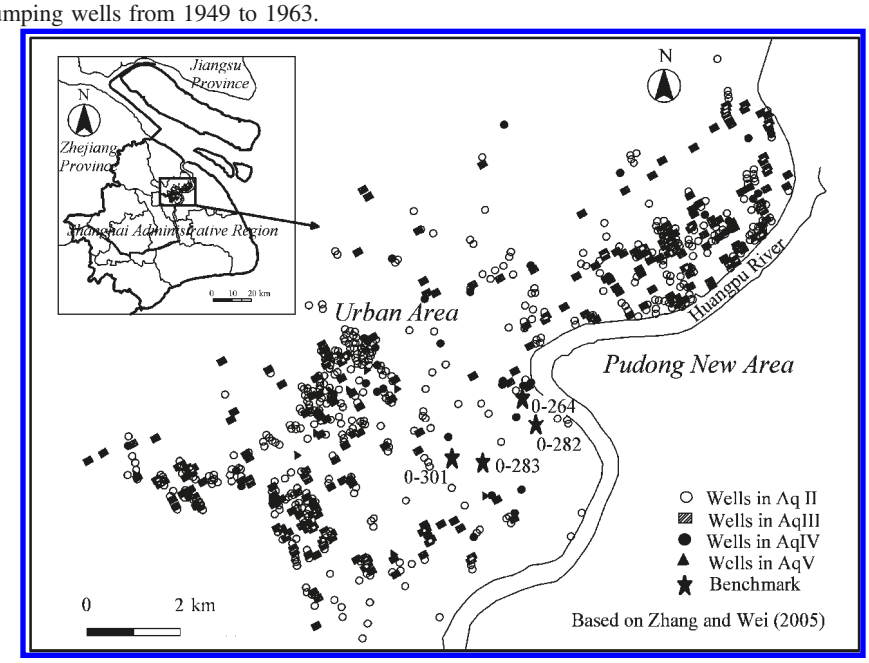

Fig. 5. Distribution of pumping wells during 1990 to 2005.

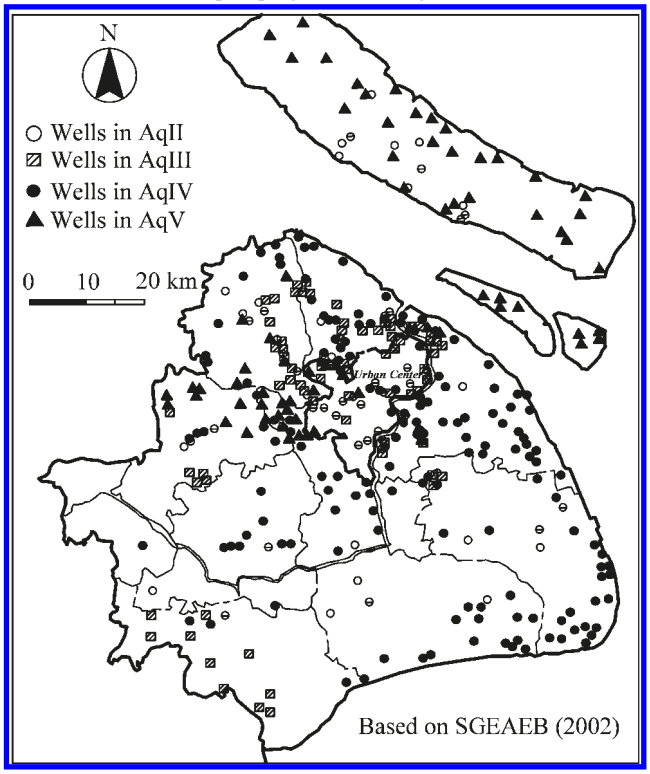

Fig. 6. Measured subsidence curves of some benchmarks in the center area of Shanghai (modified from SGEAEB 2002).

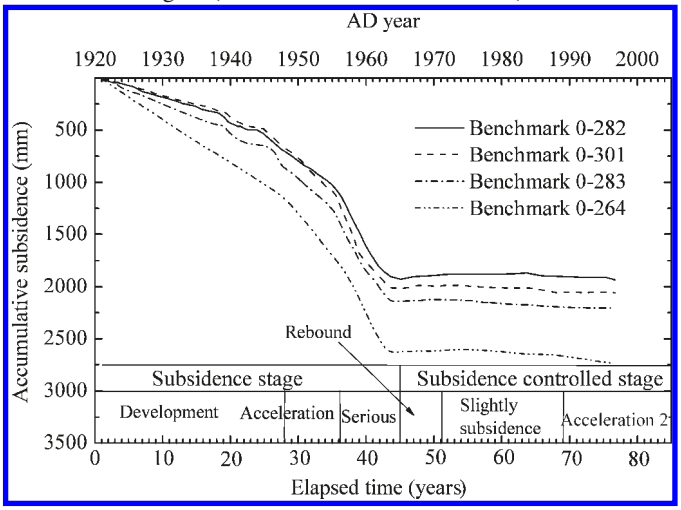

where k is the current hydraulic conductivity; C_v is the consolidation coefficient.

Variation of effective vertical stress at any elapsed time, $\Delta\sigma_z(t)$, can be calculated based on variation of groundwater head, $\Delta H(t)$, which can be calculated from eq. [7]. Therefore, the compression of soil layer, $S(t)$, at any elapsed time, t, can be expressed as a function of the hydraulic head (Shen et al. 2006)

$$[11] \qquad S(t) = m_v \Delta\sigma_z(t) H_T \approx S_s \Delta H(t) H_T$$

where, H_T is the thickness of calculated soil layer.

Thus, we can calculate the compression of soil layer with variation of the hydraulic head from the specific storage, S_s. The value of land subsidence can be calculated by accumulating the compression of soil layers.

$$[12] \qquad S_{sub} = \sum_{i=1}^{m} S(t) = \sum_{i=1}^{m} S_{si} H_{Ti} \Delta H_i(t)$$

Shen et al. (2006) compared the consolidation compression by using the aforementioned approach with the result from an oedometer test. It was confirmed that the proposed approach is suitable for solving engineering problems.

Variation of parameters in flow model

During consolidation, changes in effective stress and void ratio cause changes in consolidation parameters. Previous studies from the literature showed that, in the simulation of land subsidence induced by groundwater pumping, consider-

Fig. 7. Volume of groundwater pumped and recharged: (*a*) withdrawal; (*b*) recharge.

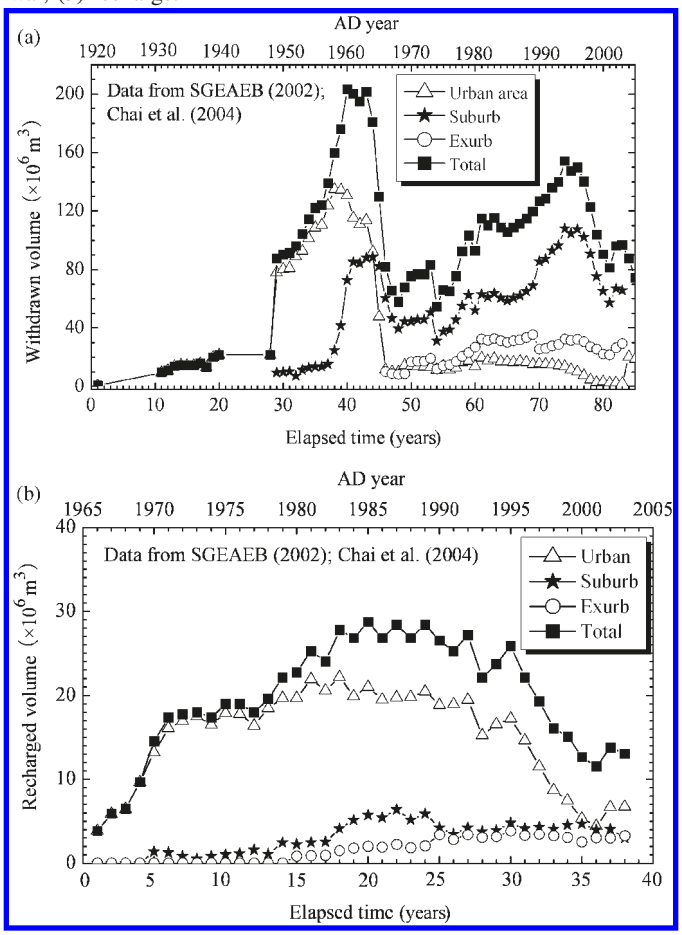

Fig. 8. Volume of groundwater pumped from each aquifer.

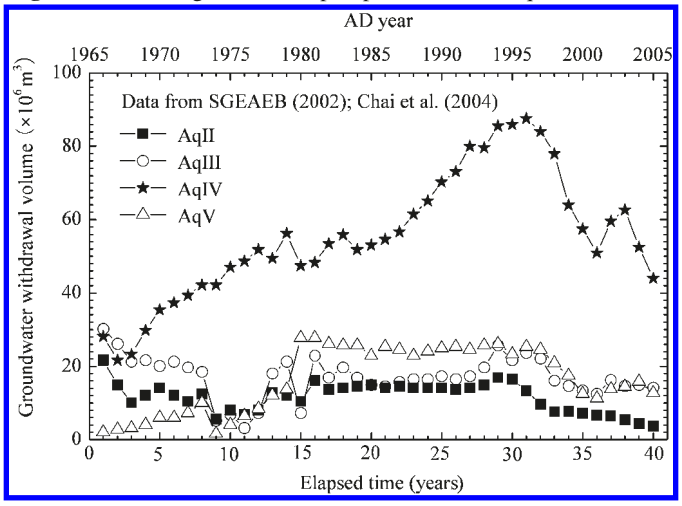

ation of the change in the hydraulic conductivity and coefficient of volume compressibility of aquitards would result in reasonable results (Neuman 1973; Helm 1976; Bethke and Corbet 1988; Rudolph and Frind 1991).

Hydraulic conductivity

The variation in hydraulic conductivity due to consolidation can be expressed as a function of void ratio. However, variation behaviors of sandy and clayey soils are different.

For clayey soils in an aquitard, hydraulic conductivity varies with void ratio, e, and is denoted by the Taylor (1948) equation as follows:

$$[13] \qquad k(e) = k_0 10^{-(e_0 - e)/C_k}$$

where k_0 is the initial hydraulic conductivity; e_0 is the initial void ratio; C_k is a constant (= $0.5e_0$) (Tavenas et al. 1986).

The hydraulic conductivity for porous media (e.g., aquifer) is influenced by following factors: particle size, composition, degree of saturation, fabric, and void ratio (Lambe and Whitman 1979). For saturated sandy soil during consolidation, particle size, composition, and degree of saturation remain constant. Change in hydraulic conductivity is only related to the void ratio, based on the Kozeny–Carman equation (Kozeny 1927; Carman 1956), the hydraulic conductivity, varied with void ratio, e, can be expressed as:

$$[14] \qquad k(e) = k_0 \left(\frac{e}{e_0}\right)^3 \left(\frac{1 + e_0}{1 + e}\right)$$

Volumetric compressibility

The coefficient of volumetric compressibility, m_v, for clayey soil in aquitards depends on the effective stress and is expressed as

$$[15] \qquad m_v = \frac{0.434C'}{(1 + e)\sigma'_v}$$

where C' is the slope of the e-log$P$ curve (when $\sigma' < P_c$, $C' = C_s$ = unloading slope; when $\sigma' > P_c$, $C' = C_c$ = compression index, where P_c is the pre-consolidation pressure); σ'_v is the vertical effective stress.

Sandy soil is in an elastic state when the change of effective stress induced by the change of groundwater level is less than its yield stress. Therefore, for sandy soil in an aquifer, the coefficient of volumetric compressibility, m_v, is considered to be a constant value, which can be calculated from Young's modulus and Poisson's ratio as follows (Budhu 2000):

$$[16] \qquad m_v = \frac{(1 + \mu)(1 - 2\mu)}{(1 - \mu)E}$$

where μ is Poisson's ratio, E is Young's modulus.

Numerical scheme

In this study, a numerical method was employed to discretize the governing equation, eq. [7]. In the numerical scheme, a finite element method (FEM) was employed to discretize the geometric range (spatial domain) and a finite difference method (FDM) was employed for temporal discretization (Shen et al. 2006). In FEM, the analyzed domain is discretized into prism elements with multifaces, including eight-noded isoparametric elements and six-noded isoparametric elements. The variable is the hydraulic potential and is set at the node. The distribution of hydraulic head in the element is calculated approximately from the node value through an interpolation function. To eliminate the residual in the domain, the Galerkin method was employed so that the interpolation function is the same as the shape function. The element matrix is developed to relate the nodal variables of

each element. The element matrices are assembled to form a set of algebraic equations that describe the entire system. In the assembling of the entire matrix, a preconditioned conjugated gradient (PCG) was used for the allocation of each node (Neuman et al. 1982; Nishigaki 2002).

In the calculated duration, time is divided into small temporal steps. In FDM, to integrate the right side of eq. [7], the center difference method is used, that is, the difference weight parameter for each time step is equal to 1/2 (Nishigaki 2002). For the specific storage matrix, the lumped matrix method was employed (Neuman 1973).

Limitation of the method

The method employed in this study works only under the following limitations: (*i*) as it only considers the soil deformation vertically (1D) and there is no 3D stress–strain relationship, it cannot consider horizontal displacement with the effect on vertical compression; (*ii*) it cannot consider the creep behavior of soft clayey soil and (or) visco-plastic behavior of soil (Yin and Graham 1994, 1996). In this study, the consolidation analysis of clay strata is based on Terzaghi's 1D consolidation theory, which assumes that soil behavior is elastic. In fact, the stress–strain relationship of clayey soil is demonstrated to be elasto-plastic and viscous in nature (Yin 1999; Yin and Zhu 1999). Yin and Graham (1999) established a 1D elastic viscoplastic model and generalized for triaxial stress states to analyze the time-dependent stress–strain behavior of soils. Furthermore, real soil deformation is in 3D. Employing Biot's 3D consolidation theory, not only the seepage can be calculated as accurately as possible, but also an elasto-plastic constitutive relationship can be incorporated into this theory. It is necessary to establish a fully coupled model considering elasto-plastic and viscous conditions of the clay soil to predict land subsidence. However, the calculation of large-scale land subsidence in a fully coupled elastic visco-plastic 3D model needs more computer resources and as accurate soil parametersl as possible. Therefore, more detailed field and laboratory investigations on soil properties at each point should be conducted, which consumes human and natural resources and becomes uneconomical. In engineering practice, it is impossible to get the geotechnical information at each point. A fully coupled elastic visco-plastic 3D model is difficult to use in practice and there are only a few applied cases as of today. For simplicity, the present method was employed and is much more cost effective.

Calculation model of land subsidence in Shanghai

Calculation range and mesh

The calculation range includes the south part of the Shanghai Administration Region (excluding Chongming Island) and some areas of Jiangsu and Zhejiang provinces, as shown in Fig. 9. The FEM mesh in the plan is set at 5 km size in the outside region (see Fig. 9). However, around the outskirts and urban areas it was set at 2.5 and 1.25 km size, respectively. Figure 10 shows the 3D FEM mesh for the modeling on the groundwater seepage and land subsidence. To check the effect of size and shape of the mesh on the numerical results, sensitive analysis is conducted through the following four schemes: (*i*) present mesh size in the centre part is small and gradually enlarged to the outer side, with element type varied from eight-noded element to six-noded element for transition; (*ii*) eight-noded elements with fine size, such as those of interior elements of the present mesh (1.25 km in horizontal direction); (*iii*) eight-noded elements with small size, such as those of interior elements of the present mesh (2.5 km in horizontal direction); (*iv*) eight-noded elements with small size, such as those of outer element elements of the present mesh (5 km in horizontal direction). The results show that the maximum difference between mesh schemes (*i*) and (*iv*) is about 10%. However, the difference among mesh schemes (*i*), (*ii*), and (*iii*) is less than 1.0%. Thus, the adopted scheme for mesh size and shape is accurate enough for MAAS of Shanghai.

Initial and boundary conditions

The phreatic water level is set as 1.0 m below the ground surface (Chai et al. 2005). Therefore, the initial hydraulic head at the top is about 2.0–3.5 m. Over the sea, the hydraulic head is the sea surface and it is set as 0.0 m. It was assumed that at 1921, the water pressure in each aquifer was the same as the static water pressure for the periphery boundary. It is difficult to determine the ground water head at the periphery because the ground water extraction activity is conducted both in Jiangsu and Zhejiang provinces. However, in this study, the concern place is in the urban center and Pudong New Development Area (PNDA). The west and north boundaries are so far that the effect is thought negligible. On the land periphery, it is set as the constant head at the ground surface.

The place of groundwater extracted at plan is shown in Fig. 9 and groundwater was extracted from AqII to AqIV at each node in the vertical direction. The withdrawn volume of groundwater at different regions from each aquifer was assumed based on Figs. 7 and 8. Then, the regionalization volume of groundwater pumped from each aquifer is evenly distributed to each node of the pumped well. The hydraulic head at each node can be calculated using the governing equation for 3D groundwater flow (see eq. [7]). The variable is the hydraulic head and is set at the node. Variation of effective vertical stress at any elapsed time can be calculated based on variation of the hydraulic head. To compare between calculated and measured results, four benchmarks 0-264, 0-282, 0-283, and 0-301 (see Figs. 4 and 9) were selected.

Soil parameters

The water table of phreatic water is 0.3–1.5 m under the ground surface, and it changes with rainfall and tide. Soil parameters (see Fig. 3) of the hydro-geological layers in the borehole J1 at Huacao (see in Fig. 1) are used in this analysis (Xu et al. 2007). Table 2 tabulates the initial values of the parameters used in the analysis. The values of hydraulic conductivity for clayey soil given in Table 2 are based on the oedometer tests and for sandy soil in the aquifer are based on the values recommended by the Shanghai Construction Committee (SCAMC 2002; Chai et al. 2005). There are no data available on the value of k_v for each aquifer layer. The AqI is a fine sand layer with an initial value of k_v of about 9×10^{-6} m/s. Based on the test results of pumping tests, hydraulic conductivity for AqII–AqV was established to be around 10^{-4} m/s. There are very few test data for the deeper

Fig. 9. Locations of groundwater withdrawal nodes in FEM mesh.

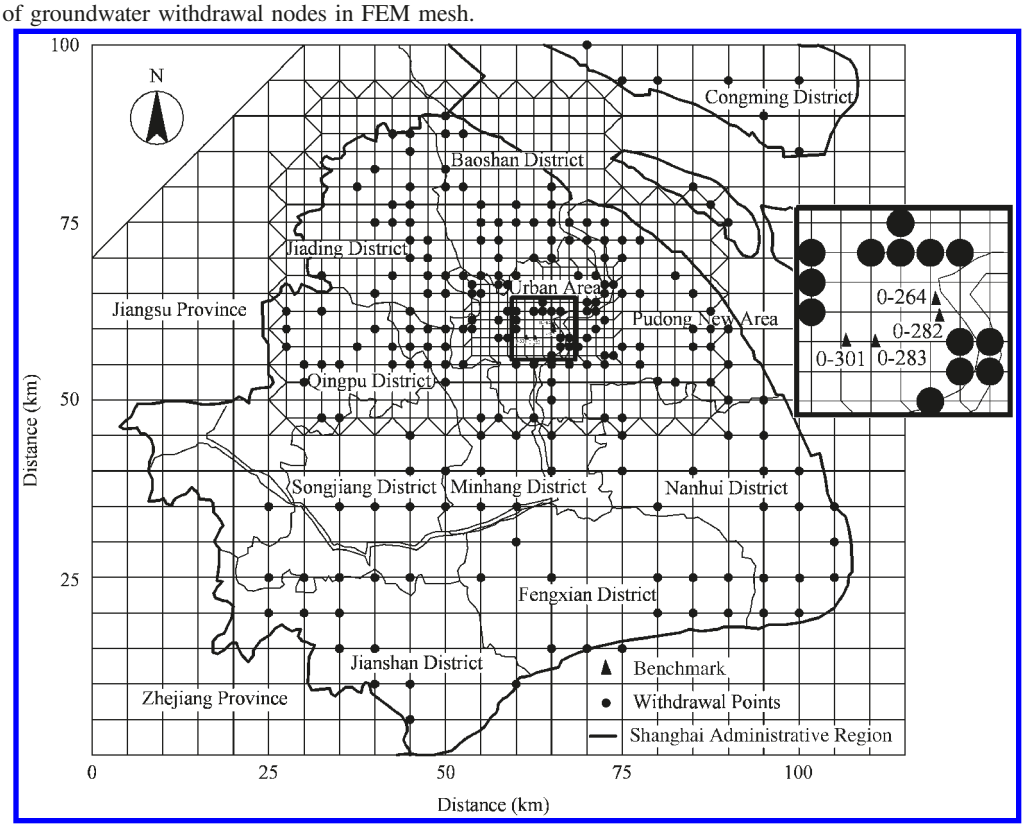

Fig. 10. 3D finite element mesh (data from Xu et al. 2007).

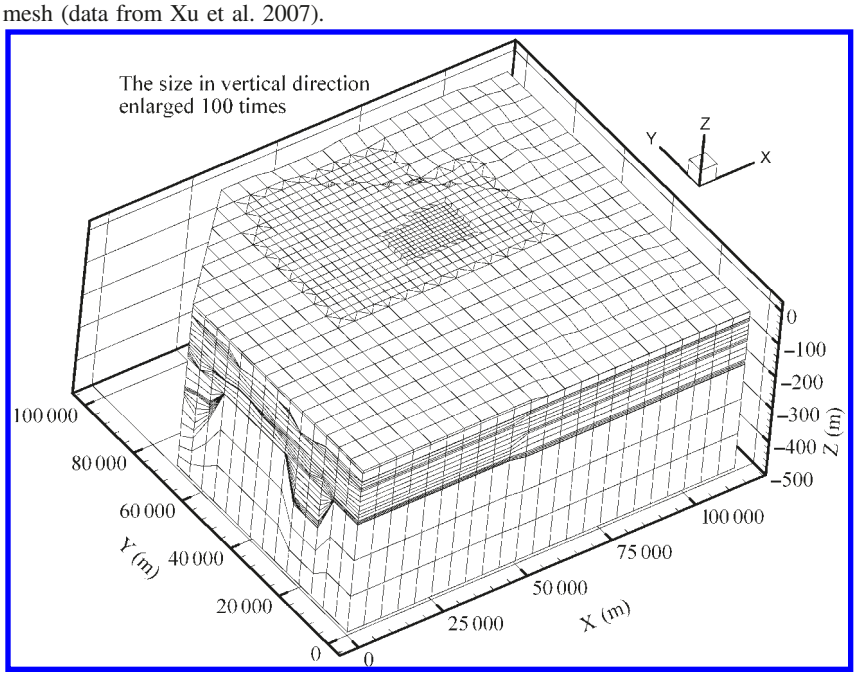

aquitards. The k_v values of the shallow aquitards were calculated from the k_v values of AdI (Chai et al. 2005). The horizontal hydraulic conductivity, k_h, is equal to 2∼3 times the vertical hydraulic conductivity, k_v. The coefficient of specific storage, S_s, at initial state is calculated from the coefficient of volumetric compressibility, m_v, as shown in eq. [9].

The initial value of m_v is determined by oedometer test at the in situ stress state of the soil layer during consolidation. During consolidation, k_v is varied with the void ratio as shown in eq. [13] for clayey soil and eq. [14] for sandy soil, m_v is varied with the in situ stress state for clayey soil as shown in eq. [15].

Table 2. Initial values of parameters used in consolidation analysis (Xu et al. 2007).

Layer	e	E (kPa)	m_v (1/kPa)	C'	k_v (m/day)	k_h (m/day)	S_s (m^{-1})
Phreatic aquifer	1.20	—	3.95×10^{-5}	0.30	4.32×10^{-3}	1.08×10^{-2}	3.75×10^{-3}
Low-pressure artesian aquifer	1.00	—	4.34×10^{-4}	0.30	4.32×10^{-3}	1.08×10^{-2}	3.75×10^{-3}
Aquitard I	1.05	—	3.52×10^{-4}	0.25	1.60×10^{-3}	4.01×10^{-3}	1.67×10^{-3}
Aquifer I	0.78	51 300	1.95×10^{-5}	—	1.04×10^{0}	2.59×10^{0}	9.67×10^{-5}
Aquitard II	0.85	—	3.28×10^{-4}	0.21	2.34×10^{-3}	5.85×10^{-3}	6.30×10^{-3}
Aquifer II	0.82	101 300	9.87×10^{-6}	—	8.64×10^{0}	2.16×10^{1}	9.67×10^{-5}
Aquitard III	0.78	—	1.95×10^{-4}	0.12	1.65×10^{-3}	4.13×10^{-3}	2.64×10^{-3}
Aquifer III	0.71	116 500	8.58×10^{-6}	—	8.64×10^{0}	2.16×10^{1}	8.41×10^{-5}
Aquitard IV	0.68	—	2.41×10^{-4}	0.14	9.85×10^{-4}	2.46×10^{-3}	2.22×10^{-3}
Aquifer IV	0.66	159 500	6.27×10^{-6}	—	8.64×10^{0}	2.16×10^{1}	6.14×10^{-5}
Aquitard V	0.62	—	1.61×10^{-4}	0.09	7.26×10^{-4}	1.81×10^{-3}	9.53×10^{-5}
Aquifer V	0.64	201 300	4.97×10^{-6}	—	8.64×10^{0}	2.16×10^{1}	4.87×10^{-5}
Aquitard VI	0.62	—	1.61×10^{-4}	0.09	7.26×10^{-4}	1.81×10^{-3}	6.90×10^{-5}

Fig. 11. Comparison between measured and calculative subsidence in Shanghai from 1920 to 2000.

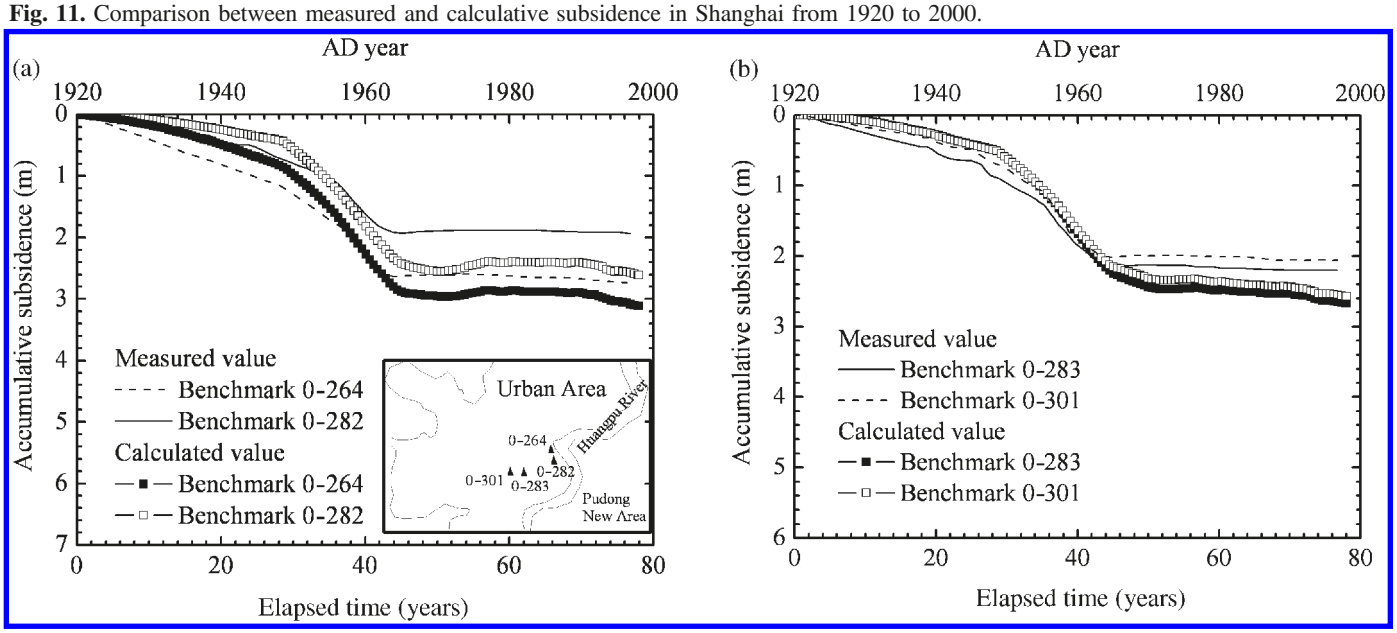

Results and discussion

Subsidence

Figure 11 shows the calculated subsidence at benchmarks 0-264, 0-282, 0-283, and 0-301 from 1920 to 2000. Before 1949, land subsidence developed slowly, and the impact on the environment was relatively small. The rate of land subsidence had increased greatly since 1949 because of the increase in the pumping volume of groundwater. The subsidence curve becomes flat after 1965, as shown in Fig. 11, as groundwater extraction was limited after 1965. Comparison between the measured and calculated values indicates that the model simulated the measured data fairly well. Figure 12 is a cumulative subsidence contour in 3D from 1920 to 2005. The discrepancies between the calculated and the measured values may be due to the following neglected factors: (*i*) limitation of the model (e.g., 3D consolidation); (*ii*) creep (elastic visco-plastic) behavior of soils; (*iii*) real distribution of wells; (*iv*) modification of soil parameters because of the existence of underground structures (Jiao et al. 2006); (*v*) urbanization-induced settlement (Xu 2010). The quantitative effects on subsidence from these factors need to be further investigated.

Groundwater level

Figure 13 depicts the drawdown of groundwater in AqII. As shown in Fig. 13, the maximum drawdown for AqII was about 1.0 m in 1921 (Fig. 13*a*). With the increase of withdrawn range and intensity of groundwater, the maximum drawdown reached 14.0 m in 1965 (Fig. 13*b*). As groundwater was recharged in 1966, the water level presents an ascending trend. In 2005, the maximum drawdown recovered to about 10.0 m (Fig. 13*c*). Figure 13 also shows that the maximum drawdown of groundwater occurs in an urban area. This result indicates that the water level variation in aquifers is closely related to the groundwater withdrawal volume and region.

Groundwater flow vector

Figure 13 also plots groundwater flow vectors in AqII in 1921, 1965, and 2005. It can be found that the groundwater flowed from west to east before 1965 (Fig. 13*a* to Fig. 13*b*),

Fig. 12. Accumulated subsiding cone and contour in 3D in 2005. Settl., settlement.

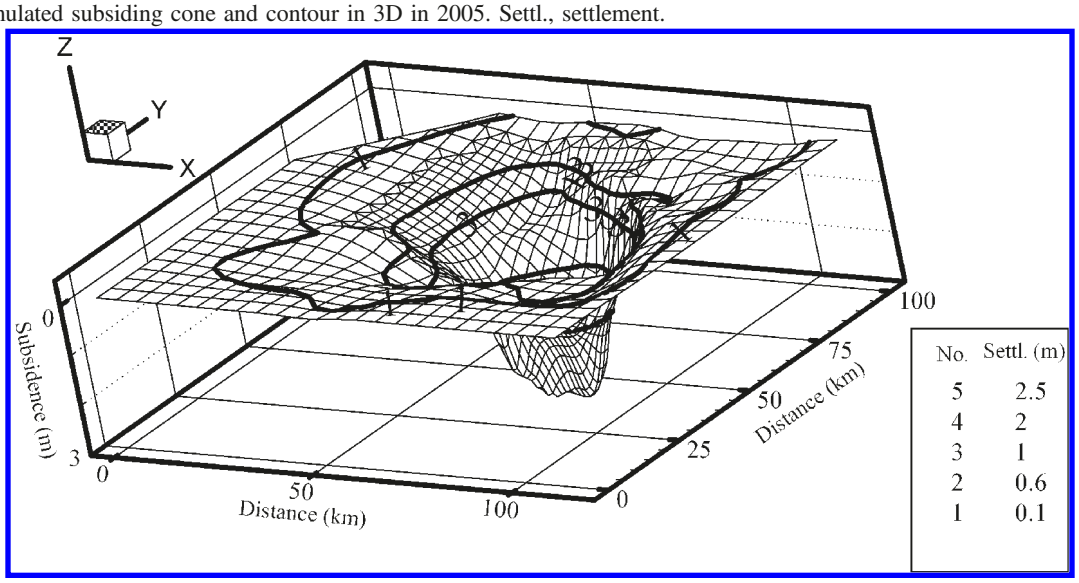

and groundwater flowed from surroundings to center in 2005 (Fig. 13*c*), indicating that the groundwater supply path changed. The natural groundwater supply in Shanghai comes from neighboring provinces (e.g., Jiangsu and Zhejiang provinces). After long-term groundwater pumping, the replenishment of groundwater comes from groundwater reservoirs of the East China Sea continental shelf, and groundwater flows from land and sea to urban areas. The replenishment area has been enlarged accompanied by the groundwater withdrawal volume and region. This simulated result is consistent with the field-observed phenomena (Lu 1994).

Groundwater flow vectors of other aquifers (AqIII–AqV) are plotted in Fig. 14. Groundwater flow trends in these three Aquifers are similar to that in AqII. The most different groundwater flow is in the Jinshan District because of different geological conditions, in which some outcrops exist.

Prediction of future behavior

To predict the future behavior of subsidence, the scenarios (see Table 3) are assumed by considering the following changes: (*i*) volume of withdrawn and recharged groundwater; (*ii*) pumping layer; (*iii*) pumping region (urban to suburban and coastal area), in which more attention was paid to the subsidence development in Pudong New Area. The prediction to 2035 is based on the pattern of groundwater pumping and recharge in 2005. The pumping and recharge in 2005 was already presented in the previous publication (Xu et al. 2007). Groundwater withdrawal volume was 0.745×10^8 m^3 and groundwater recharge volume was 0.150×10^8 m^3 in 2005 and thereby the net withdrawal volume was 0.595×10^8 m^3. The detailed groundwater withdrawal volume and subsidence of different prediction plans as listed in Table 4.

Control of withdrawn–recharged volume of groundwater

Plan 1-1: Maintaining withdrawn–recharged volume of 2005

This plan keeps the well location and follows the withdrawal and recharge volume from 2005. Figure 15 shows the predicted subsidence at benchmarks from 2006 to 2035. Because withdrawal and recharge volumes are kept constant during this period, subsidence increases linearly. If land subsidence was controlled as 28.7 mm/a, the calculated net withdrawal volume would be 0.595×10^8 m^3. The predicted result for allowable withdrawn volume is approximately equal to the value estimated by the field observed result (Shen et al. 2005). Shen et al. (2005) proposed a method to predict the allowable withdrawal volume of groundwater in a special geological condition. This statistical method is based on the field data of groundwater recharge and observed land subsidence under the condition without groundwater recharge before 1965. However, this statistical method based on regression analysis is not applicable to predict net withdrawal volume in the future. Thus, the numerical model shows its power to predict future behavior. Figure 16 shows the predicted cumulative subsidence contour in 2035. The maximum accumulated subsidence reaches 1.2 m, which occurs in the Pudong New Area, whereas the land subsidence in urban areas ranges from 0.5 to 1.0 m. Figure 17 shows groundwater flow vectors and contour of groundwater drawdown for AqII in 2035. Replenishment sources include groundwater both from urban and surrounding areas.

Plan 1-2: Maintaining recharged volume but reducing withdrawn volume

In this plan, groundwater recharged volume remains constant, equal to 0.150×10^8 m^3. The withdrawn volume decreases by 5%/a and reaches 0.21×10^8 m^3 in 2035. The maximum land subsidence takes place in Pudong New Area and reaches 0.4 m.

Plan 1-3: Maintaining withdrawn volume but increasing recharged volume

In this plan, groundwater withdrawn volume remains constant, equal to 0.745×10^8 m^3, and recharged volume is increased by 5%/a and reaches 0.51×10^8 m^3 in 2035. The maximum land subsidence takes place in Pudong New Area and reaches 0.75 m.

Figure 18 shows the predicted subsidence of benchmark 0-283 of plan 1 in Shanghai from 2006 to 2035. It is shown that the decrease of groundwater withdrawn volume or in-

Fig. 13. Groundwater flow vectors and contour of groundwater drawdown for AqII in (*a*) 1921; (*b*) 1965; (*c*) 2005.

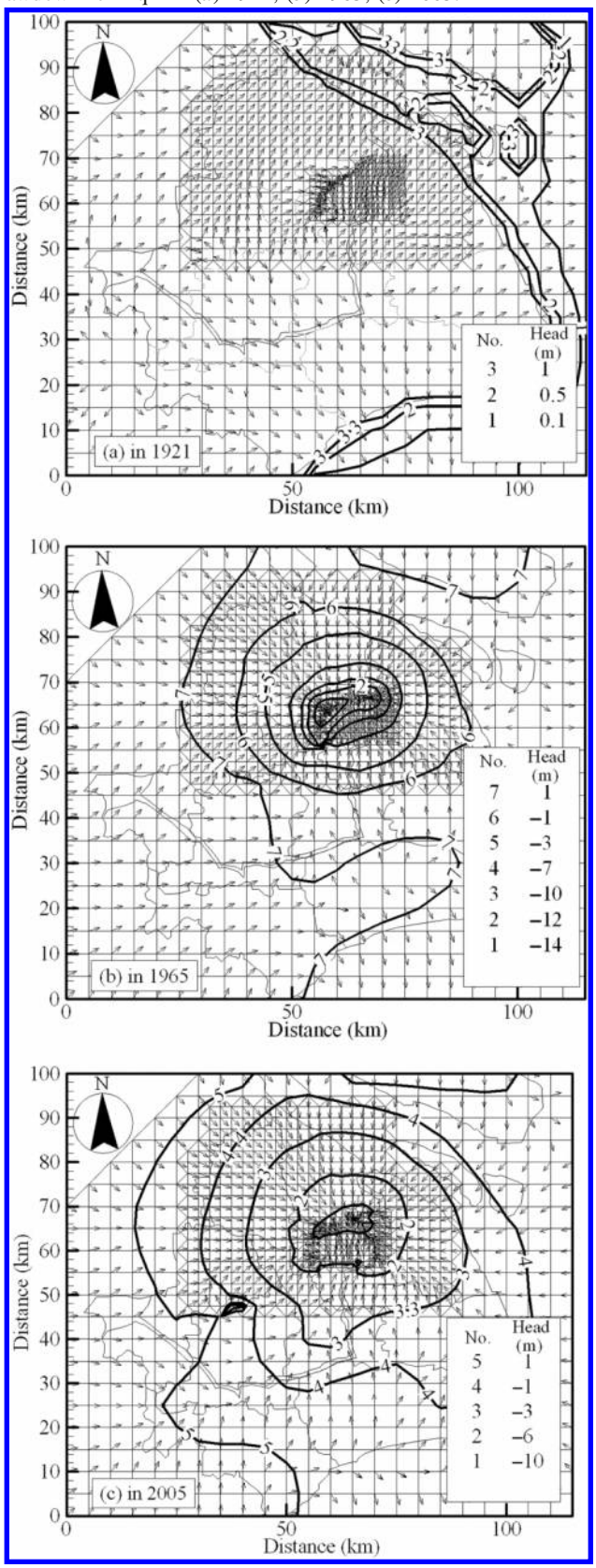

Fig. 14. Groundwater flow vectors and contour of groundwater drawdown in 2005: (*a*) AqIII; (*b*) AqIV; (*c*) AqV.

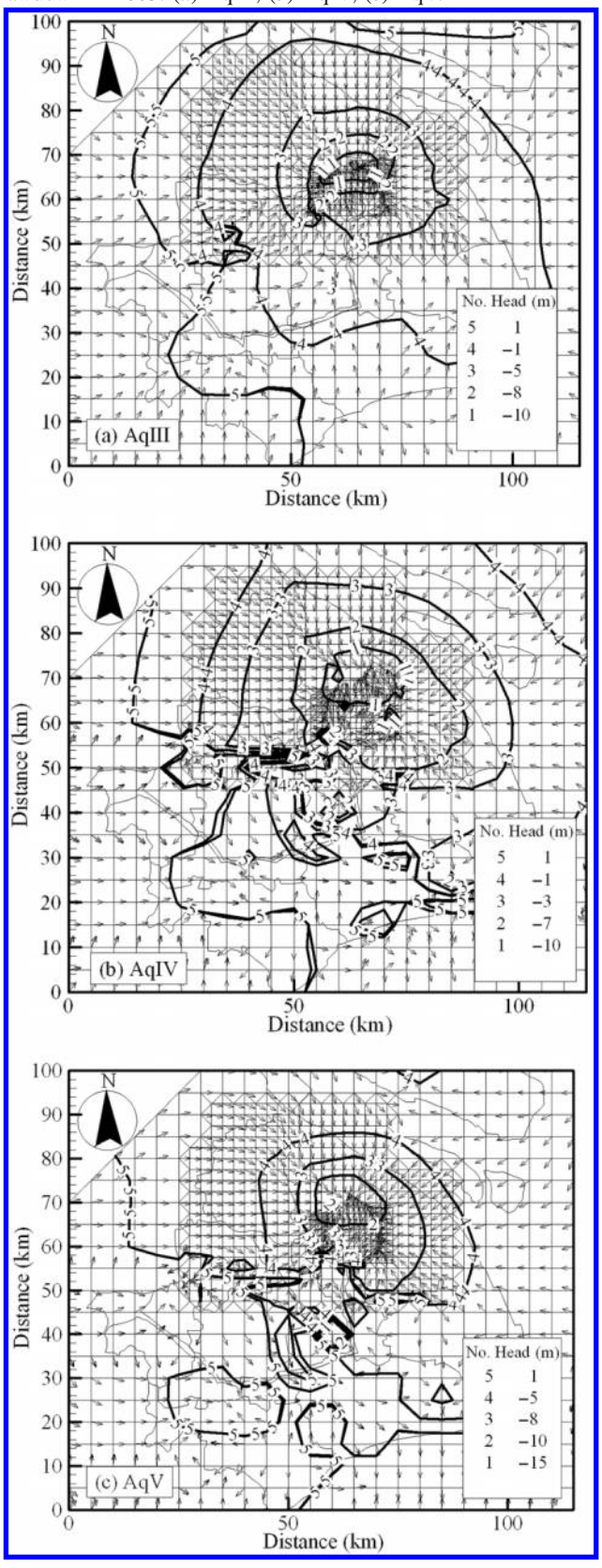

Table 3. Assumed scenarios in prediction of future behaviors of subsidence.

Scenario	Plan	Content descriptions
1: Groundwater withdrawn–recharged volume	1-1	Keeping withdrawn–recharged volume of 2005
	1-2	Keeping recharged volume but changing withdrawn volume
	1-3	Keeping withdrawn volume but changing recharged volume
2: Shifting groundwater pumping layer	2-1	Groundwater withdrawn–recharged in Aquifer II and III
	2-2	Groundwater withdrawn–recharged in Aquifer IV and V
	2-3	Groundwater recharge in Aquifer II and III and groundwater withdrawal in Aquifer IV and V
3: Changing groundwater pumping region	3	Withdrawn wells allocated along the coastal regions

Table 4. Comparison of predicted subsidence from different plans.

		Groundwater withdrawn volume ($\times 10^8$ m^3) in 2030					Groundwater recharged volume ($\times 10^8$ m^3) in 2030					
Prediction scenario	Plan	AqII	AqIII	AqIV	AqV	Total	AqII	Aq III	AqIV	AqV	Total	Accumulative subsidence at benchmark 0-283 in 25 years (m)
Plan 1	1-1	0.037	0.119	0.454	0.134	0.745	0.104	0.036	0.011	0.000	0.15	0.749
	1-2	0.011	0.034	0.128	0.038	0.21	0.104	0.036	0.011	0.000	0.15	0.106
	1-3	0.037	0.119	0.454	0.134	0.745	0.352	0.122	0.036	0.000	0.51	0.079
Plan 2	2-1	0.373	0.373	0	0	0.745	0.075	0.075	0	0	0.15	0.720
	2-2	0	0	0.373	0.373	0.745	0	0	0.075	0.075	0.15	0.765
	2-3	0	0	0.373	0.373	0.745	0.075	0.075	0	0	0.15	0.686
Plan 3	3	0.037	0.119	0.454	0.134	0.745	0.104	0.036	0.011	0.000	0.15	0.566

Fig. 15. Predicted subsidence of benchmarks in Shanghai from 2006 to 2035 (plan 1-1).

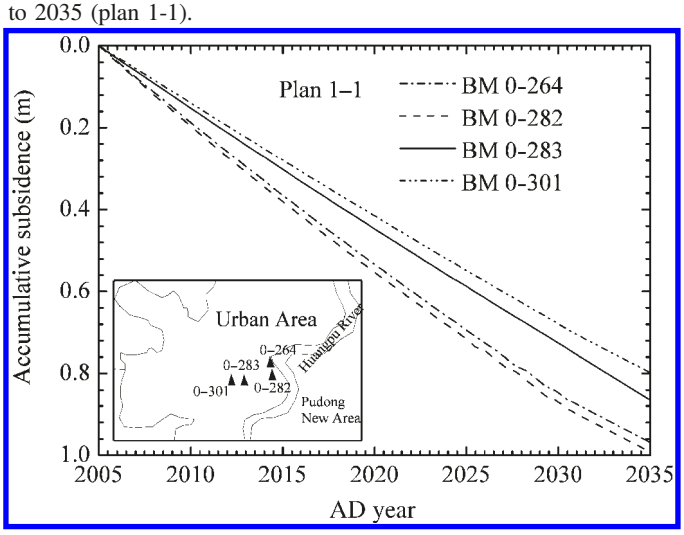

Fig. 16. Predicted cumulative subsidence contour in 2035 (plan 1-1).

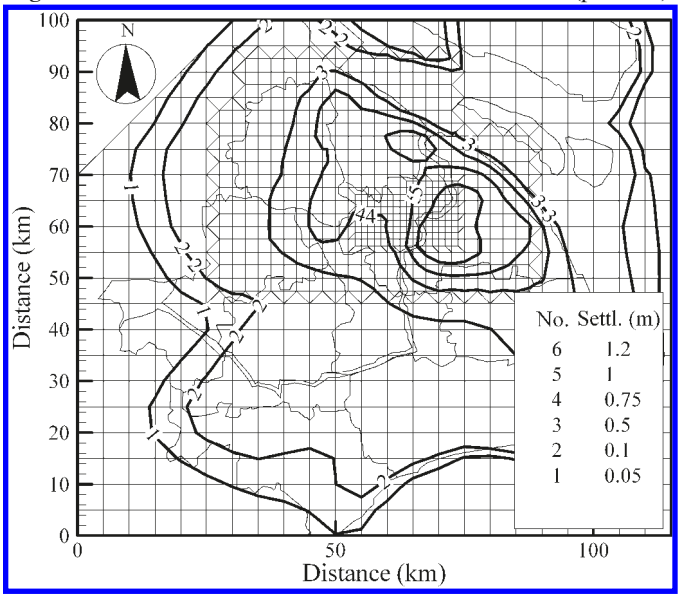

crease of recharged volume can mitigate land subsidence. From Fig. 18, it can also be found that, after 2025, some rebound happened in plans 1-2 and 1-3. Moreover, plan 1-2 results in the smallest subsidence whereas plan 1-1 results in largest subsidence.

Shifting groundwater pumping layer

Plan 2-1: Groundwater withdrawn–recharged in AqII and AqIII

In this plan, the ratio of groundwater withdrawn–recharged volume in AqII to that in AqIII is one to one. Groundwater withdrawn volume is 0.373×10^8 m^3, and recharged volume is 0.075×10^8 m^3 in AqII and AqIII, respectively. AqIV and AqV have no groundwater withdrawal and recharge.

Plan 2-2: Groundwater withdrawn–recharged in AqIV and AqV

In this plan, the ratio of groundwater withdrawn–recharged volume in AqIV to that in AqV is one to one. Groundwater withdrawn volume is 0.373×10^8 m^3, and recharged volume was 0.075×10^8 m^3 in AqIV and AqV, respectively. AqII and AqIII have no groundwater withdrawal and recharge.

Fig. 17. Groundwater flow vectors and contour of groundwater drawdown for AqII in 2035 (plan 1-1).

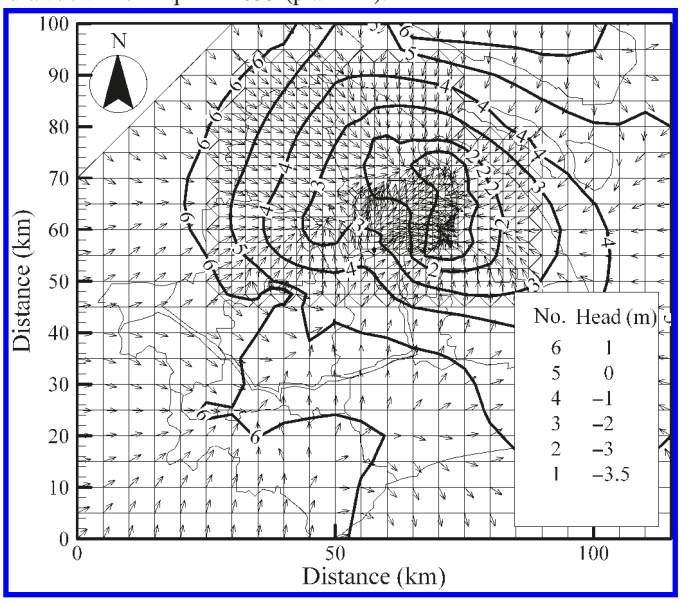

Fig. 18. Predicted subsidence in Shanghai from 1999 to 2035 (plans 1-1–1-3 and plans 2-1–2-3).

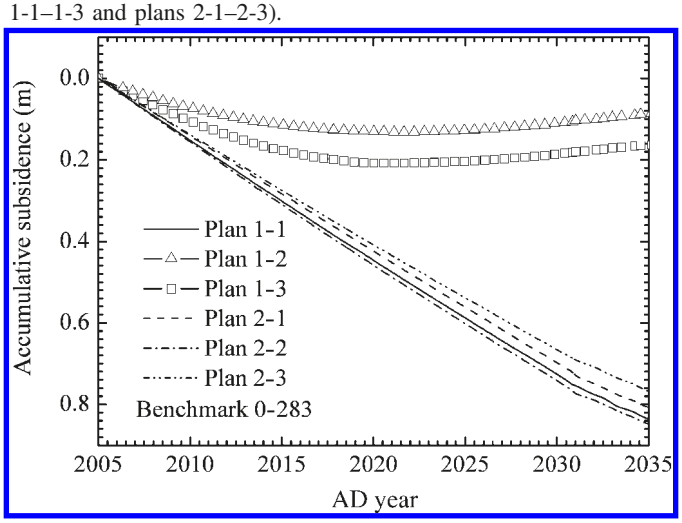

Plan 2-3: Recharge in AqII and AqIII and withdrawal in AqIV and AqV

In this plan, the ratio of groundwater withdrawal volume in AqIV to that in AqV is one; the ratio of recharged volume in AqII to that in AqIII is one. The groundwater withdrawn volume is 0.373×10^8 m^3 in AqIV and AqV, and recharged volume is 0.075×10^8 m^3 in AqII and AqIII.

Figure 18 also shows the predicted subsidence of benchmark 0-283 of plan 2 in Shanghai from 2006 to 2035. It can be seen that the land subsidence of plan 2-2 is larger than that of plan 2-1. This observation indicates that groundwater withdrawal and recharge only in AqIV and AqV will not mitigate the land subsidence. It is clearly shown that the land subsidence of plan 2-3 is the smallest among these three plans, indicating that recharge in AqII and AqIII and withdrawal in AqIV and AqV is a good idea to mitigate land subsidence.

Changing groundwater pumping region

Plan 3: Wells moving to coastal regions

This plan keeps withdrawal–recharge volume and pumping aquifers but changes the location of withdrawn wells. According to the calculated result in plan 1, the maximum subsidence occurs in the Lujiazui Area, which is the economical center of Shanghai. In the Lujiazui Area, the land subsidence must be controlled to a very small value. Therefore, plan 3 assumes that the pumping wells move to the coastal region, as shown in Fig. 19. Two points (point A, which is out of the withdrawal area; and point B, which is within the withdrawn area) are selected for the comparison with plan 1-1. Land subsidence at these two points in plan 3 are both larger than plan 1-1, while subsidence of benchmark 0-283 in plan 3 is smaller than that in plan 1-1, as shown in Fig. 20. Figure 21 shows the predicted cumulative subsidence contour in 2035, and Fig. 22 shows the groundwater flow vectors and drawdown contour of AqII in 2035. In plan 3, the maximum subsidence happens in the withdrawn area, and the subsiding area is smaller than that with plan 1-1. That is because of the replenishment of seawater. This can also be observed from Fig. 21. The groundwater replenishment area includes urban and withdrawal areas, which is different from plan 1.

The calculated result indicates that the countermeasures for subsidence control in Shanghai include change of pumping layer and adjustment of withdrawn region. However, if the withdrawal well is allocated in the coastal region, seawater will flow into land area to supply groundwater, which will exacerbate the groundwater quality and cause seawater intrusion and (or) coastal erosion.

Conclusions

A finite element calculation model is established to estimate land subsidence due to withdrawal of groundwater in Shanghai. The model is an integrative model and considers 3D groundwater seepage and 1D consolidation. The following conclusions can be drawn:

1. The model considers the formation of the MAAS of the soft deposit of Shanghai. The model simulates the variation of the coefficient of volumetric compressibility and hydraulic conductivity with the consolidation process. The calculated value of land subsidence using the proposed model simulates the measured value fairly well.
2. The results indicate that groundwater flowed from land to sea before 1965, while groundwater flowed from sea to land in 2005, indicating that the replenishment sources of groundwater changed. This may cause seawater intrusion hazards.
3. The simulated results show that there exists an obvious drawdown cone of groundwater head in urban regions of Shanghai. The maximum drawdown of groundwater head was about 14 m after 45 years since 1921. The groundwater recharge starting from 1966 mitigates the drawdown of the water table.
4. In the case that land subsidence is controlled within 28.7 mm, it is suggested that the net withdrawal groundwater volume is about 0.595×10^8 m^3 in urban areas.
5. Both reducing withdrawal volume and increasing recharged volume can control land subsidence. However, to satisfy

Fig. 19. Allocation of pumping wells from 2006 to 2035 (plan 3).

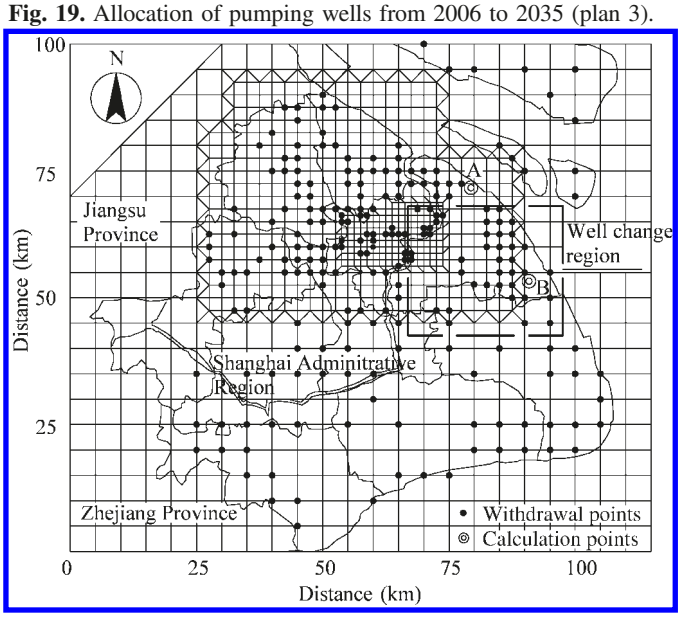

Fig. 20. Predicted subsidence in Shanghai from 2006 to 2035 considering reallocation of wells.

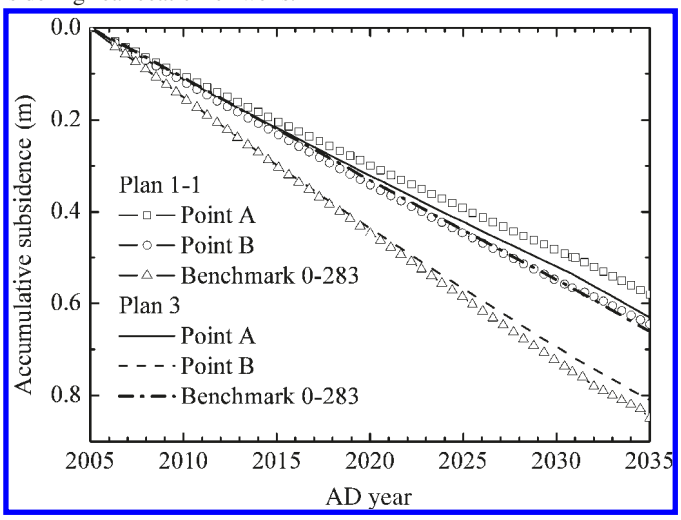

the requirement of groundwater for industrial use in Shanghai, it is impossible to reduce groundwater withdrawal volume dramatically so it is better to increase the recharged volume.

6. Changing groundwater withdrawn–recharged layers is an effective way to control land subsidence. This change can be conducted through withdrawal in AqIV and AqV and recharge in AqII and AqIII.
7. Even if the pumping wells move to a suburb region, subsidence will still occur in the urban center. One of the reasons for this is the reduction of replenishing water from surroundings.

Acknowledgements

The research work described herein was funded by the National Nature Science Foundation of China (NSFC) (Grant Nos. 41072209 and 41102175) and the joint research program between NSFC and the Japan Society for the Promotion of Science (JSPS) (Grant no. 50911140105). This work is a part of the second author's Ph.D. dissertation and this study was financially supported by Funding of Exceptional Ph.D. dissertation of the Graduate School of Shanghai Jiao Tong University. This financial support is gratefully acknowledged.

Fig. 21. Predicted accumulative subsidence contour in 2035 (plan 3).

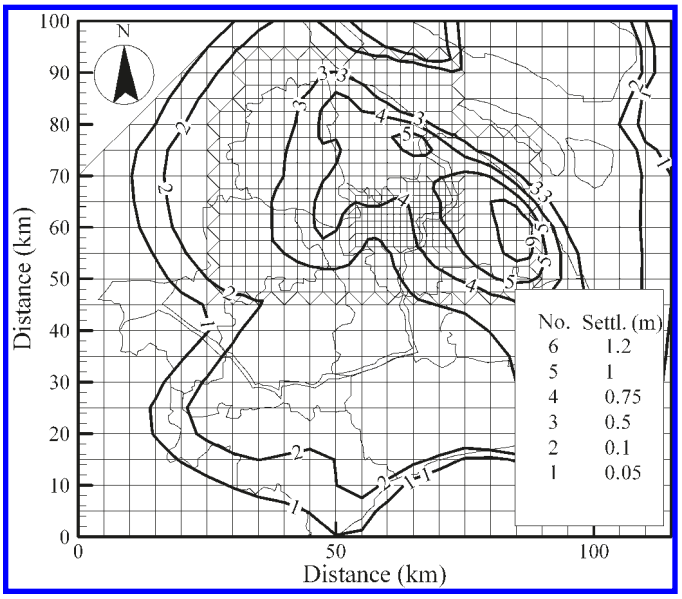

Fig. 22. Groundwater flow vector and drawdown contour of groundwater for AqII in 2035 (plan 3).

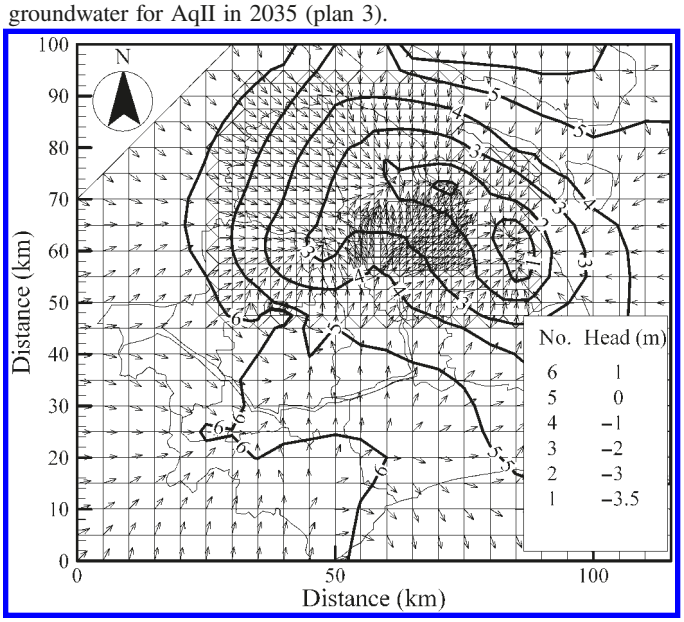

References

Bear, J. 1979. Hydraulics of groundwater. McGraw-Hill, New York.

Bethke, C.M., and Corbet, T.F. 1988. Linear and nonlinear solution for one-dimensional compaction flow in sedimentary basin. Water Resources Research, **24**(3): 461–467. doi:10.1029/WR024i003p00461.

Budhu, M. 2000. Soil mechanics and foundations. John Wiley & Sons, Inc., New York.

Carman, P.C. 1956. Flow of gases through porous media. Academic Press, New York.

Chai, J.C., Shen, S.L., Zhu, H.H., and Zhang, X.L. 2004. Land subsidence due to groundwater drawdown in Shanghai. Géotechnique, **54**(2): 143–147. doi:10.1680/geot.2004.54.2.143.

Chai, J.C., Shen, S.L., Zhu, H.H., and Zhang, X.L. 2005. 1D analysis of land subsidence in Shanghai. Lowland Technology International, **7**(1): 33–41.

Gambolati, G., and Freeze, R.A. 1973. Mathematical simulation of the subsidence of Venice: 1. Theory. Water Resources Research, **9**(3): 721–733. doi:10.1029/WR009i003p00721.

Giao, P.H., and Ovaskainen, E. 2000. Preliminary assessment of Hanoi land subsidence with reference to groundwater development. Lowland Technology International, **2**(2): 17–29.

Gong, S.L. 2009. Variation of seepage condition in aquifers of Shanghai with the effect of the development of land subsidence. Journal of Water Resources and Engineering, **20**(3): 1–6. [In Chinese.]

Harada, K., and Yamanouchi, T. 1983. Land subsidence in the Saga Plain, Japan, and its analysis by the quasi-three-dimensional aquifer model. Geotechnical Engineering, **14**(1): 23–54.

Helm, D.C. 1976. One-dimensional simulation of aquifer system compaction near Pixley, California: 2, Stress-dependent parameters. Water Resources Research, **12**(3): 375–391. doi:10.1029/WR012i003p00375.

Holzer, T.L., and Bluntzer, R.L. 1984. Land subsidence near oil and gas fields, Houston, Texas. Ground Water, **22**(4): 450–459. doi:10.1111/j.1745-6584.1984.tb01416.x.

Jiao, J.J., Wang, X.S., and Nandy, S. 2006. Preliminary assessment of the impacts of deep foundations and land reclamation on groundwater flow in a coastal area in Hong Kong, China. Hydrogeology Journal, **14**(1–2): 100–114. doi:10.1007/s10040-004-0393-6.

Kozeny, J. 1927. Ueber kapillare leitung des wassers im boden. Akademie der Wissenschaften, Wien, **136**(2a): 271–306.

Lambe, T.W., and Whitman, R.V. 1979. Soil mechanics. SI Version. John Wiley & Sons, New York.

Li, Q.F., Fang, Z., and Wang, H.M. 2000. A mathematical model and forecast of groundwater workable reserves for Shanghai. Shanghai Geology, (2): 36–43. [In Chinese.]

Lu, Z.J. 1994. Distribution of the confined fresh-water aquifer in Shanghai and its extension to the sea. Shanghai Geology, (1): 1–12. [In Chinese.]

Neuman, S.P. 1973. Saturated-unsaturated seepage by finite elements. Journal of the Hydraulics Division, ASCE, **99**(12): 2233–2250.

Neuman, S.P., Preller, C., and Narasimhan, T.N. 1982. Adaptive explicit-implicit quasi three-dimensional finite element model of flow and subsidence in multiaquifer systems. Water Resources Research, **18**(5): 1551–1561. doi:10.1029/WR018i005p01551.

Nishigaki, M. 2002. Analysis of groundwater flow in saturated-unsaturated porous media via FEM. Association of Groundwater, Okayama, Japan. [In Japanese.]

Qian, S.Y., and Gu, X.Y. 1981. Computation of land subsidence in Shanghai. Chinese Journal of Geotechnical Engineering, **3**(3): 1–9. [In Chinese.]

Rudolph, D.L., and Frind, E.O. 1991. Hydraulic response of highly compressible aquitards during consolidation. Water Resources Research, **27**(1): 17–30. doi:10.1029/90WR01700.

SCAMC. 2002. Standard for geotechnical investigation in Shanghai. Shanghai Construction and Management Commission (SCAMC), Shanghai, China. [In Chinese.]

SGEAEB. 2002. Shanghai Geological Environmental Atlas. Shanghai Geological Environmental Atlas Editorial Board (SGEAEB), Geology Press, Beijing, China.

SGO. 1976. Report on land subsidence in Shanghai (1962–1976). Shanghai Geology Office (SGO), Shanghai, China. [In Chinese.]

SGO. 1979. Hydrogeological map of Shanghai, No. 45 Hydrogeological Atlas of China. Shanghai Geology Office (SGO). *Edited by* the Institute of Hydrogeology and Engineering Geology (IHEG), China Geology Bureau, China Map Publisher, Beijing, China.

Shen, S.L., Xu, Y.S., Tang, C.P., and Cai, Z.Y. 2005. A method to determine the allowable withdrawn volume of groundwater based on annual land subsidence and pumping rate. China Patent Number: ZL200510110425.9. [In Chinese.]

Shen, S.L., Xu, Y.S., and Hong, Z.S. 2006. Estimation of land subsidence based on groundwater flow model. Marine Georesources and Geotechnology, **24**(2): 149–167. doi:10.1080/10641190600704848.

Shi, X.Q., Wu, J.C., Ye, S.J., Zhang, Y., Xue, Y.Q., Wei, Z.X., Li, Q.F., and Yu, J. 2008. Regional land subsidence simulation in Su-Xi-Chang area and Shanghai City, China. Engineering Geology, **100**(1–2): 27–42. doi:10.1016/j.enggeo.2008.02.011.

Tavenas, F., Tremblay, M., Larouche, G., and Leroueil, S. 1986. In situ measurement of permeability in soft clays. *In* Proceedings of the ASCE Specialty Conference: Use of In Situ Tests in Geotechnical Engineering, Blacksburg, Va., 23–25 June 1986. GSP 6. *Edited by* S. P. Clemence. Geotechnical Engineering Division of the American Society of Civil Engineers (ASCE), New York. pp. 1034–1048.

Taylor, D.W. 1948. Fundamentals of soil mechanics. John Wiley & Sons Inc., New York.

Terzaghi, K. 1925. Erdbaumechanik auf Bodenphisikalischer Grundlage. Franz Deuticken, Wien (Vienna), Austria.

Xu, Y.S. 2010. Evaluation of the behavior of groundwater seepage and land subsidence via considering infrastructures inserted in aquifers. Ph.D. dissertation, Shanghai Jiao Tong University, Shanghai, China. [In Chinese.]

Xu, Y.S., Shen, S.L., Hayashi, S., and Cai, Z.Y. 2007. Analysis on groundwater withdrawal and land subsidence in Shanghai. Lowland Technology International, **9**(2): 2–7.

Xu, Y.-S., Shen, S.-L., Cai, Z.-Y., and Zhou, G.-Y. 2008. The state of land subsidence and prediction approaches due to groundwater withdrawal in China. Natural Hazards, **45**(1): 123–135. doi:10.1007/s11069-007-9168-4.

Xu, Y.S., Shen, S.L., and Du, Y.J. 2009*a*. Geological and hydrogeological environment in shanghai with geohazards to construction and maintenance of infrastructures. Engineering Geology, **109**(3–4): 241–254. doi:10.1016/j.enggeo.2009.08.009.

Xu, Y.-S., Zhang, D.-X., Shen, S.-L., and Chen, L.-Z. 2009*b*. Geohazards with characteristics and prevention measures along the coastal regions of China. Natural Hazards, **49**(3): 479–500. doi:10.1007/s11069-008-9296-5.

Yin, J.-H. 1999. Non-linear creep of soils in oedometer tests. Géotechnique, **49**(5): 699–707. doi:10.1680/geot.1999.49.5.699.

Yin, J.H., and Graham, J. 1994. Equivalent times and one-dimensional elastic viscoplastic modelling of time-dependent stress-strain behaviour of clays. Canadian Geotechnical Journal, **31**(1): 42–52. doi:10.1139/t94-005.

Yin, J.H., and Graham, J. 1996. Elastic visco-plastic modelling of one-dimensional consolidation. Géotechnique, **46**(3): 515–527. doi:10.1680/geot.1996.46.3.515.

Yin, J.H., and Graham, J. 1999. Elastic visco-plastic modelling of the time-dependent stress-strain behavior of soils. Canadian Geotechnical Journal, **36**(4): 736–745. doi:10.1139/t99-042.

Yin, J.H., and Zhu, J.G. 1999. Elastic visco-plastic consolidation modelling and interpretation of porewater pressure responses in clay underneath Tarsiut Island. Canadian Geotechnical Journal, **36**(4): 708–717. doi:10.1139/t99-041.

Zhang, A.G., and Wei, Z.X. 2005. Land subsidence in China. Shanghai Scientific and Technical Press, Shanghai, China. [In Chinese.]